Visible light active C-doped titanate nanotubes prepared *via* alkaline hydrothermal treatment of C-doped nanoparticulate TiO_2: Photo-electrochemical and photocatalytic properties.

Elaine M. Neville[a], J. M. Don MacElroy[b], K. Ravindranathan Thampi[b*] and James A. Sullivan[a*]

[a] SFI Strategic Research Cluster in Solar Energy Conversion, UCD School of Chemistry and Chemical Biology, UCD Science Centre, University College Dublin, Belfield, Dublin 4, Ireland

[b] SFI Strategic Research Cluster in Solar Energy Conversion, UCD School of Chemical and Bioprocess Engineering, University College Dublin, Belfield, Dublin 4, Ireland

Corresponding authors.

james.sullivan@ucd.ie, Tel: +35317162135, Fax:+35317162127

ravindranathan.thampi@ucd.ie, Tel: +35317161995, Fax: +35317162127

Abstract

Carbon-doped titanate nanotubes (C-TNT) were formed *via* alkaline hydrothermal treatment of a TiO_2 nanoparticulate material pre-doped with carbon. Attempts to form C and W co-doped titanate nanotubes using analogous C and W co-doped nanoparticulate materials were unsuccessful. Physical characterisations, such as X-ray diffraction, N_2 physisorption and Transmission Electron Microscopy, confirmed the formation of titanate nanotubes ~7 nm in diameter and hundreds of nm in length with increased surface areas relative to the nanoparticulate precursors. X-ray Photoelectron Spectroscopy confirmed the retention of substitutional carbon dopant and the exclusion of tungsten dopant from the doped TNT materials.

Converting doped (or undoped TiO_2) into C-TNT (or TNT) slightly increases the material's bandgap but the C-TNT material (in contrast to TNT and undoped TiO_2) absorbs into the visible region of the spectrum. C-doped and un-doped titanate nanotube materials were more active in promoting the photo degradation of 4-chlorophenol under visible light than their analogous nanoparticulate precursors. C-TNT was the most photocatalytically active material tested.

However, photocurrent response measurements showed C-TNT to be less effective at generating current following irradiation than both its nanoparticulate analogue and nanoparticulate P25 when screen printed onto electrode surfaces. We ascribe this to non-optimal alignment of the TNTs on the electrode surface.

Keywords: doped titanate nanotubes, hydrothermal synthesis, photocatalysis, photo-electrochemistry

1 Introduction

The formation of titanate (TiO_2) nanotubes (TNT) by simple hydrothermal methods was first demonstrated by Kasuga *et al.* [1, 2]. Since then, TNTs have attracted much interest especially in the field of photocatalysis [3]. Various synthesis techniques have been explored to form TNTs and TNT arrays such as electrochemical anodic oxidation, *e.g.* see [4, 5] and assisted–templating, *e.g.* see [6, 7]. However, hydrothermal synthesis remains one of the most facile formation procedures [2, 8-11].

The exact structure of hydrothermally derived TNTs is currently disputed [12], but they are generally referred to as protonated titanate or TiO_2 nanomaterials [1, 3]. It has been reported that the nanotubes have a $H_2Ti_3O_7$ structure [13] that is formed by rolling up the [010] direction of single-layers of $H_2Ti_3O_7$ peeled off from a $H_2Ti_3O_7$ crystal sheet [9] formed during hydrothermal treatment of TiO_2. The rolling is thought to occur due to hydrogen deficiency in surface layers [9] or due to mechanical stress [14]. Other reports claim that the tubes are of anatase TiO_2 structure [1, 15, 16] and are formed by rolling single-layer TiO_2 nanosheets.

TNTs potentially offer enhanced photocatalytic efficiencies compared with conventional nanoparticule TiO_2 systems. Due to their nanotube structure (~8 nm diameter, ~100 – 200 nm length [1, 2]), they have higher adsorption capacities (due to higher surface areas which can be 400 $m^2 g^{-1}$ [1]), enhanced electron transfer and more efficient e^- / h^+ charge separation [17] relative to nanoparticulate systems. Therefore they may display increased photocatalytic ability.

However, the major limitation associated with the use of all Ti-containing materials (either nanoparticulate TiO_2 or TNTs) as solar-driven photocatalysts is that the band gap is too large for visible light to promote an electron from the valance band to the conduction band (to initiate photocatalysis). Recently much research has focused on selective doping of both metallic and non-metallic elements (such as carbon and nitrogen) into the lattice of TiO_2 nanoparticles in an attempt to shift absorbance into the visible region of the solar spectrum and so increase the number of utilizable solar photons available for initiation of photocatalysis [18-24]. Doping of TNTs (with elements such as carbon, nitrogen or tungsten) might further enhance the photocatalytic efficiencies of the nanotube materials by similarly extending the absorption onset into the visible light region [25-27].

Most doped titanate nanotubes synthesised using the facile hydrothermal approach have been formed *via* hydrothermal treatment of a dopant source and undoped TiO_2 together. For example, nitrogen-doped titanate nanotubes have been formed *via* hydrothermal treatment of urea with an undoped TiO_2 source [28]. Doped Titanate nanotubes have also been formed *via* treatment of the prepared nanotubes with a dopant source, *e.g.* N-doped titanate nanotubes have been formed *via* heat treatment of titanate nanotubes in a flow of NH_3 [29].

Similar approaches have been used to incorporate C-dopants into TNT arrays grown from a Ti substrate by anodization. Addition of carbon sources to the electrolyte [30 during TNT growth, as well as annealing un-doped TNT arrays at high temperature under a flow of CO [31] or C_2H_2 [32]. Co-doped nanotubes have also been prepared and applied, but their modes of synthesis have involved combinations of the *in-situ* and post modification techniques described above [33, 34].

Efforts to dope nanoparticulate TiO_2 have also included the two approaches above, *i.e.* treatment of pure TiO_2 with a dopant-containing molecule at high temperature and the (far more flexible and controllable) wet chemistry approach using modified sol-gel syntheses [35]. This work describes attempts to use the straightforward controllable doping associated with modified sol-gel syntheses in combination with the facile hydrothermal formation of titanate nanotubes to generate doped titanate materials.

To our knowledge, such a preparation of doped TNTs synthesised *via* hydrothermal treatment of a pre-doped nanoparticulate materials has not been previously reported. Given the range of doped materials that can be prepared through modified sol-gel processing, this approach might open a straightforward and reproducible route to the formation of a large number of variously doped titanate nanotubes.

Doped TiO_2 materials were first formed through hydrolysis of $TiCl_4$ in the presence of melamine borate (the source of carbon dopant) [35] and, in the case of C,W-co-doped materials, tungstic acid [24]. These pre-doped TiO_2 materials were then subjected to a standard hydrothermal treatment [13] to form doped titanate nanotubes (Figure 1).

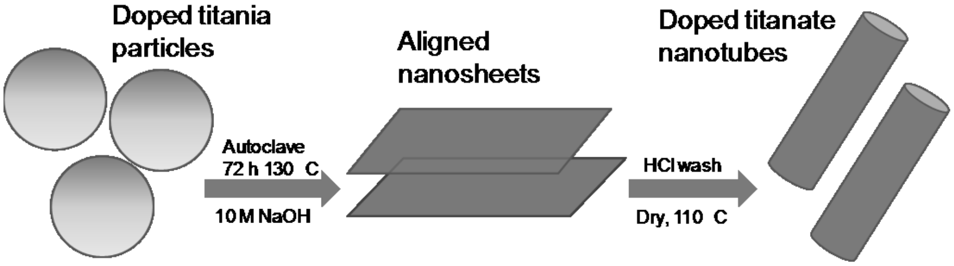

Figure 1. Doped TNTs formed *via* hydrothermal treatment of doped TiO_2 particles

Once formed, the materials were characterised using a range of analysis techniques, including transmission electron microscopy (TEM), X-Ray diffraction (XRD), N_2 physisorption and X-ray photoelectron (XPS) and UV-Vis spectroscopies. Finally, TNT materials were applied in photocatalysis and photoelectrochemistry.

2 Experimental

Doped nanoparticulate TiO_2 materials, as well as P25 (Degussa), were used as precursor materials for the synthesis of various titanate nanotubes. Titanate nanotubes (TNTs) were formed using P25 as the precursor. A carbon-doped titanate nanotube (C-TNT) was formed using C-TiO_2 as a precursor. Attempts to form carbon and tungsten co-doped titanate nanotubes (C,W-TNT) involved the use of nanoparticulate C,W-TiO_2 as a precursor.

2.1 Doped anatase particulate TiO_2

Doped TiO_2 materials were synthesised by hydrolysis of $TiCl_4$ (followed by condensation) to form $X_3Ti\text{-}O\text{-}TiX_3$ lattices (where X represents OH or -O-TiX_3 groups). In the case of C-doped catalysts the carbon was derived from melamine borate which was added to the mixture prior to hydrolysis [35]. Melamine is particularly resistant to calcination and calcinations can be carried out at 400 °C and above while still retaining a portion of the dopant. Tungsten doping was introduced through the addition of tungstic acid to the mixture [24].

In a typical synthesis of C-doped TiO_2 (C-TiO_2) 3.4 g of melamine borate (Budenheim, Germany) was dissolved in 0.5 L deionised water under constant stirring at room temperature. After 24 h, the solution was filtered through Whatman Grade 1 filter paper. 11 mL $TiCl_4$ ($\geq$ 99.0 % (AT), Fluka) was slowly dissolved in 1.5 L of deionised water at 2 – 4 ºC. To this solution 14 mL of melamine borate solution were added and stirred for 30 minutes. A 2.5 M solution of ammonium hydroxide (made through dilution of a 26 % solution, Riedel-de Haen, Germany) was added drop-wise until pH 5 was reached. This resulted in precipitation of the TiO_2 precursor from the solution. The precipitate obtained was allowed to settle overnight before being filtered through Whatman Grade 1 filter paper and washed repeatedly with warm de-ionised water (to eliminate Cl^- from the solid). The removal of Cl^- was confirmed using a standard $AgNO_3$ precipitation test. The solid was then dried at 80 ºC overnight. The resultant material was ground into fine powder and calcined at 400 °C for 1 h. Similarly, a W, C co-doped material was prepared using the addition of 1% tungstic acid (99 %, Aldrich) within the precipitating mixture [24] (C,W-TiO_2).

2.2 Titanate nanotubes

Titanate nanotubes were synthesised by the hydrothermal treatment of a TiO_2 powder. 1 g of photocatalyst powder (P25 TiO_2 (Degussa)) was added to 50 mL of a 10 M NaOH solution and digested at 130 °C for 72 h in a Teflon lined steel autoclave. Following this treatment the material is reported to exist as an aligned nanosheet [36]. The white precipitate was filtered and washed with dilute HCl and distilled water. This process reportedly forms open-ended titanate nanotubes which were then dried at 110 °C overnight and calcined at 380 °C for 2 h.

Attempts were made to form doped titanate nanotubes by replacing the TiO_2 powder used above with previously prepared doped TiO_2 powders. This process was carried out using previously synthesised C-TiO_2 and C,W-TiO_2 powders.

2.3 Photoelectrochemical characterisation

In order to evaluate photoelectrochemical characteristics of the catalysts, electrodes were formed from these powders. Pastes of various photocatalyst powders were first fabricated according to the procedure set out by Ito *et al.* [37]. The pastes were then used to deposit thin layers (measured using ellipsometry to be approximately 1.2 μm thick) of the TiO_2 materials onto conducting substrates *via* screen printing.

Photocurrent density, under light on/off illumination, was measured to confirm the photo-responses of photoelectrodes during potential sweeps. The measurements of photocurrent were carried out using a custom made photoelectrochemical (PEC) cell, a Gamry G300 potentiostat and a Newport 450W (xenon arc lamp) solar simulator providing a AM 1.5 G spectrum. The PEC cell consisting of three electrodes, the working electrode (photoelectrode), counter electrode and a reference electrode, saturated calomel electrode (SCE), was immersed in an electrolyte aqueous solution of 1 M NaOH (pH ~13) which was degassed by purging with 99.99 % pure N_2 and mechanically stirred during the experiments. The cell had a flat fused glass window to facilitate illumination of the photoelectrode thin film surface.

2.4 Photocatalytic activity

The photocatalytic activity of the materials was tested by investigating the degradation of 4-chlorophenol solutions in the presence of the photocatalyst powders under illumination. Typically 80 mg of photocatalyst powder was dispersed in 40 mL of a 0.5 mM solution of 4-chlorophenol. The mixture was sonicated for 15 minutes before being purged with air for 5 minutes. Samples were stirred in the dark for 60 minutes. This has been found to be sufficient to achieve an adsorption – desorption equilibrium between the reactant and the catalyst surface [38]. Irradiation was carried out in an Atlas Suntest CPS+ solar simulator unit containing a 1500 Watt Air Cooled Xenon Arc Lamp. The solar simulator unit provides an AM 1.5 G spectrum [50] and was used in conjunction with a UV filter film ($\lambda > 410$ nm). The degradation (complete mineralisation) of 4-chlorophenol was monitored using Total Organic Carbon (TOC) analysis (Shimadzu TOC V-CPH).

2.5 Characterisation techniques

Powder XRD patterns were collected using a Siemens D500 Kristalloflex using Cu Kα radiation. N_2 physisorption isotherms were collected using a Quantachrome Nova 2000e. Diffuse Reflectance UV-Vis spectroscopy (DRS) was carried out with an Analytik Jena Specord 210 spectrometer equipped with an integrating sphere attachment for measurement of spectra from powder samples. X-ray Photoelectron Spectroscopy (XPS) was carried out with a Kratos AXIS 165 spectrometer using a monochromatic X-ray source (Al Kα 1486.58 eV). A Tecnai 20 Transmittance Electron Microscope (TEM) was used to image the nanostructured materials.

3 Results and Discussion

3.1 X-ray diffraction

The crystal structure of titanate nanotubes derived from hydrothermal synthesis is controversial [3]. Initially reports claimed that the nanotubes are anatase in structure [1, 2]. However, more recently the general consensus has been that the structure is not so straightforward [3].

Various titanate or TiO_2 crystallographic structures have been proposed (see Table 1). There are many reasons for the difficulty in conclusively characterising nanotubes crystallographically. One is that their structure is relatively unstable and the can undergo further phase transformation, for example during heating [39] or acid treatment [40], during or after preparation, resulting in the wide variety of structures reported.

Crystallographic phase *	XRD reflection 2θ (°)									
nanotubes	10.5		24.4	28	34	38.5	44.5	48.2		61.5
$H_2Ti_3O_7$	11		24.4	29	33	38		48.4	60	62
$H_2Ti_2O_4(OH)_2$	9		24.3	28	34	38		48		62
$H_2Ti_4O_3.H_2O$	10		24	28				48		
$H_xTi_{2-x/4}\square_{x/4}O_4.H_2O$	9.5		24.5	28				48		62
TiO_2.B		15	25	29.5			44	48	57	62
$H_2Ti_3O_{11}.H_2O$	10	14			36		43	46		

Table 1. Examples of proposed nanotube crystal phases and the corresponding XRD reflections (2°) as reviewed by Bavykin *et al.* [3] * □ indicates a vacancy

Another difficulty in characterising these materials crystallographically is that the XRD patterns of the hydrothermally derived nanotubes are low in intensity with broad peaks that are difficult to interpret and assign. This may be due to low crystallinity, small crystal sizes or due to the nature of the nanotube formation (reportedly, if the pre-nanotube nanosheet wraps along a certain crystallographic axis it results in the broadening of the peak of the given Miller indices [3]). Many of the proposed titanate or TiO_2 structures display XRD reflections at very similar 2θ° values (see Table 1), making them difficult to distinguish from one another.

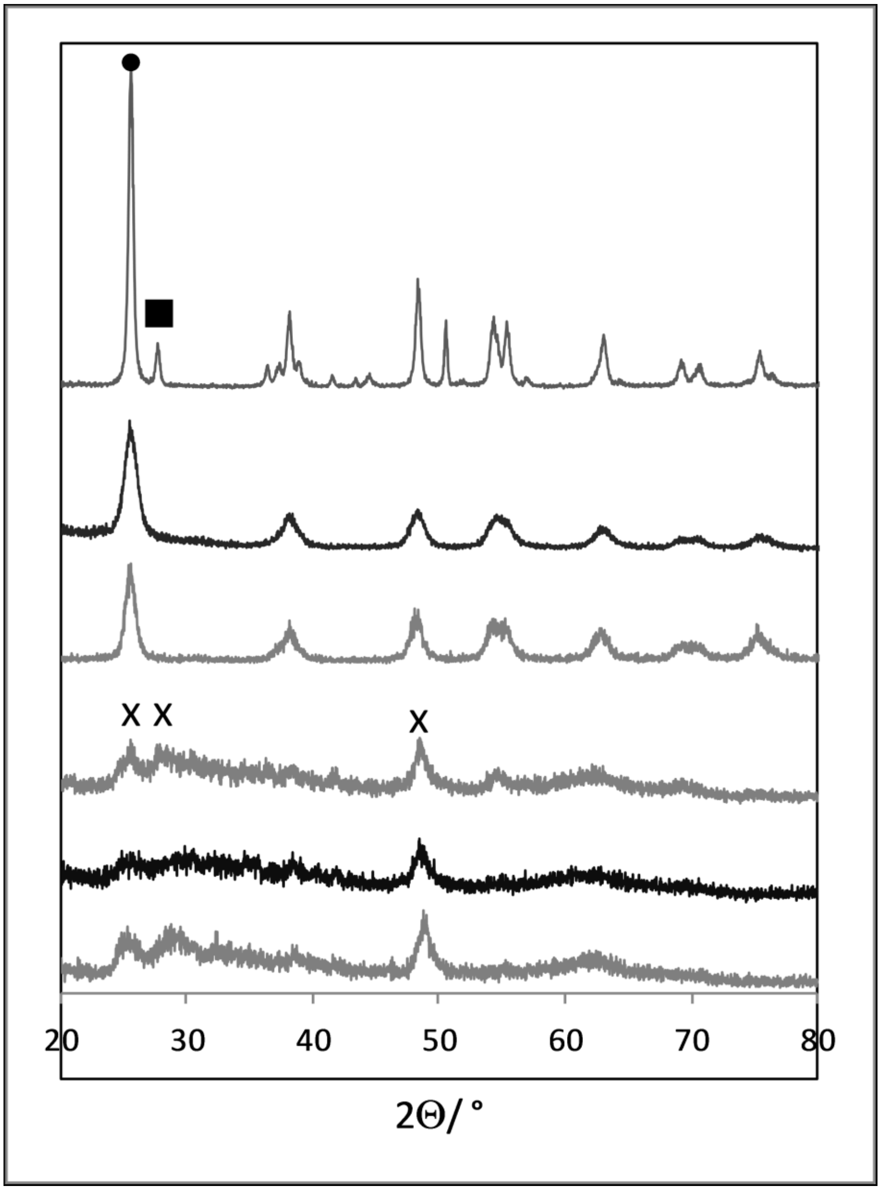

Figure 2. XRD patterns of P25, C-TiO_2, (both decreased to 33% of intensity), C,W-TiO_2, C,W-TNT, C-TNT and TNT

Despite the difficulties surrounding the definitive crystallographic characterisation of these materials, the TNTs formed here were analysed using XRD and patterns relating to TNT, C-TNT and C,W-TNT are shown in Figure 2. Profiles relating to P25, C-TiO_2 (both with intensities decreased by a factor of 3) and C,W-TiO_2 (the nanoparticulate precursor materials) are also shown for comparison. P25 displays a mixture of both anatase (JCPDS 21-1272) and rutile phase peaks (JCPDS 21-1276). The (101) anatase peak and (110) rutile peak are shown by ● and ■ respectively. C-TiO_2 and C,W-TiO_2 both displayed only anatase phase peaks. The XRD patterns of the various TNT materials are dominated by a peak at $2\theta = \sim 50°$ confirming titanate-type formation. Other peaks at $2\theta = \sim 24°$ and $2\theta = \sim 26°$ observed in the TNT XRD patterns (shown by X) are also related to a titanate-type structure [41].

This confirms that after hydrothermal treatment in 10 M NaOH, followed by washing with HCl and water, and calcination at 380 °C, the materials have undergone a significant change in crystal structure (*i.e.* before treatment the particulate materials displayed anatase and rutile peaks but after hydrothermal treatment all TNT materials displayed only titanate-phase peaks). Dopant incorporation into the nanoparticulate precursor has not noticeably affected the resultant XRD patterns. However, for the reasons discussed above, it is difficult to confirm whether any major differences are present.

One clear difference between the doped and undoped titanate samples is that, notwithstanding the fact that all the titanate profiles suggest relatively poorly crystalline phases, the phase formed from P25 seems a little more crystalline (with narrower and more defined peaks) than those formed from the doped TiO_2 precursors. Given that all three materials underwent the same chemical and thermal treatment; this suggests the presence of the dopants affects the crystallinity of the formed titanate nanotubes.

3.2 N_2 physisorption

N_2 physisorption was used to determine the surface areas of the materials. Typical BET profiles of the TNT and C-TNT materials are shown in the supplementary information document. Table 2 shows the surface areas of TNT, C-TNT and C,W-TNT along with their nanoparticulate precursors (P25, C-TiO_2, C,W-TiO_2). All of the TNT materials tested displayed a significant increase in surface area, compared to that of their nanoparticulate precursors. C-TNT and C,W-TNT had a higher surface area than TNT. This feature most likely relates to the larger surface areas of their respective nanoparticulate TiO_2 analogues (C-TiO_2 and C,W-TiO_2) relative to P25. This, in turn, arises due to differences in nucleation and particle growth during the sol-gel process when nanoparticualtes are formed.

	Nanoparticle surface area (m^2 g^{-1})	**Titanate surface area (m^2 g^{-1})**	**Pore volume (mL g^{-1})**	**Pore radius (nm)**	**Pore diameter (nm)**
P25	55.6	110.3	0.6	1.6	3.2
C-TiO_2	148.2	162.2	0.6	1.6	3.2
C,W-TIO_2	104.5	161.7	0.5	1.4	2.9

Table 2. Textural data as determined by N_2 physisorption using the BET and BJH methods (volume, radius and diameter data relate to the relevant nanotube materials)

However, the difference in surface area seen in the precursors between C-TiO_2 and C,W-TiO_2 is not reflected in the surface areas of the nanotubes these materials form. The BJH method was applied to determine pore volumes and pore radii of the TNT materials and the results from these calculations are also reported in Table 2.

3.3 *Diffuse reflectance UV-Vis spectroscopy*

Diffuse reflectance UV-Vis spectroscopy was used to determine the opto-electronic properties of the TNT materials. Figure 3 shows the UV-Vis spectra of TNT, C-TNT, C,W-TNT and P25 (Degussa)). TNT and P25 (Degussa) were white in colour, while C-TNT and C,W-TNT were a very pale yellow. This is suggestive of absorbance in the visible region (with absorbance of violet light causing the material to appear yellow).

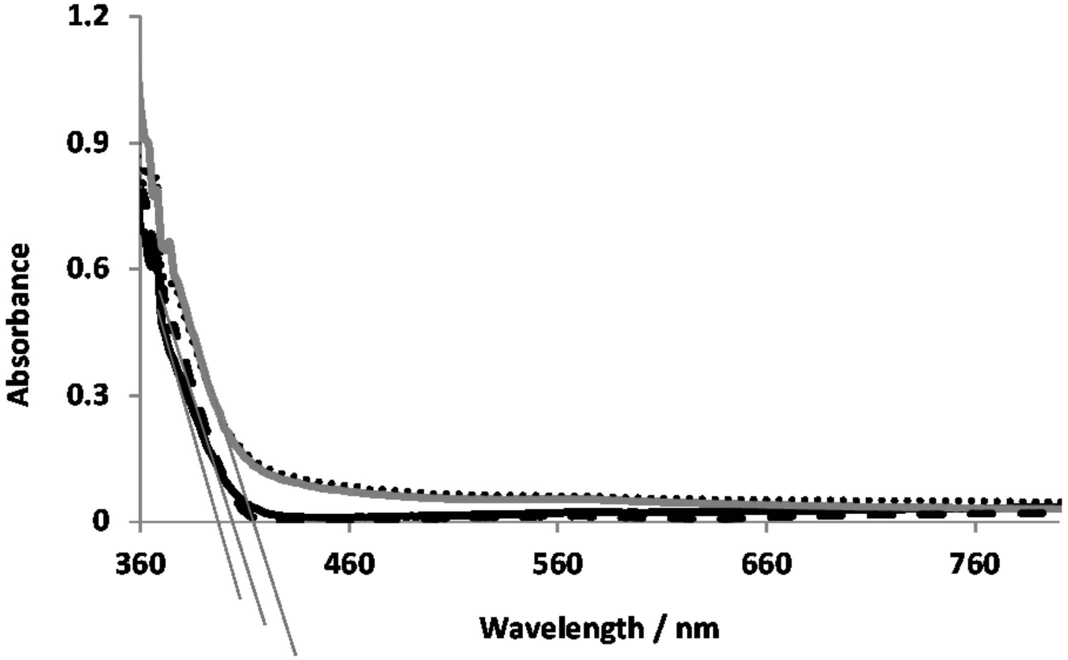

Figure 3 UV-Vis spectra of TNT (black line), C-TNT (dotted line), C,W-TNT (grey line) and P25 (dashed line)

Absorbance onsets were estimated by drawing a tangent to the high-energy feature of the UV-Vis spectrum and approximating the wavelength at which the tangent intercepts a line with an absorbance value of zero. TNT and P25 (Degussa) displayed absorbance onsets at 405 and 410 nm respectively (resulting in calculated band gaps of 3.02 and 3.06 eV respectively). TNT type materials display a decrease in absorbance onset (and increase in band gap) relative to nanoparticulate TiO_2 due to hydration and nano-size effects [42]. C-TNT and C,W-TNT displayed improved absorbance onsets relative to both TNT and P25. This is suggestive of dopant incorporation into the titanate structure [26, 43].

Band gaps were estimated from the absorbance onsets (Table 3) using $E_g = hc/\lambda$, where E_g is the band gap energy (J), h is Planck's constant, c is the velocity of light, and λ is the wavelength (m) of absorption onset. The C-TNT and C,W-TNT materials, which displayed a red shift in optical absorbance relative to P25 and TNT, were both estimated to have band gaps of 2.95 eV. These values are lower than the band gap estimations for P25 and TNT (3.02 eV and 3.06 eV, respectively).

	Before nanotube formation		**After nanotube formation**	
	Abs (nm)	Bandgap (eV)	Abs (nm)	Bandgap (eV)
P25	410	3.02	405	3.06
C-TiO_2	425	2.92	420	2.95
C,W-TIO_2	435	2.85	420	2.95

Table 3. Absorbance onsets (Abs) and estimated band gaps (Bg) of TNT and TiO_2 analogue materials – see [35] for measurements of nanoparticulate bandgaps.

C-TNT displayed a slight decrease in absorbance onset (and increase in calculated band gap) relative to its nanoparticulate analogue C-TiO_2 (Table 3) [35]. As mentioned above, this may be due to the change is structure from TiO_2 to hydrated titanate or, in part, to some loss of dopant during hydrothermal treatment and nanotube formation. C,W-TNT displayed an even larger decrease in absorbance onset relative to its nanoparticulate analogue C,W-TiO_2 (Table 3) and again this may reflect the change in crystal structure as well as possible loss of dopant during hydrothermal treatment and nanotube formation.

C,W-TNT displays a very similar absorbance spectrum (and calculated band gap) to C-TNT, despite the significant differences in absorptions seen in their respective nanoparticulate precursors (Table 3). This may be due to loss of the entire concentration of W, rendering C,W-TNT essentially the same as C-TNT in terms of optical properties (see XPS below).

3.4 X-ray photoelectron spectroscopy

X-ray photoelectron spectroscopy (XPS) was used to probe the presence and retention of dopants (seen to be present in the different precursor TiO_2 materials [35]) within the TNT materials.

The C 1s regions of the XPS profiles were first studied to investigate the presence of carbon dopant. Initially, samples displayed three peaks at binding energies of ~285, ~286 and ~289 eV. The peak at 285 eV is an instrumental artefact related to elemental adventitious carbon [44] present in all XPS measurements. The peaks at 286 and 289 eV have previously been related in the literature to interstitial carbonate dopants as well as oxidised carbon species adsorbed on the surface of the material [45-47]. As these peaks were found to be present in all samples, including P25, it is thought that they relate to carbon contaminants on the surface of the samples *e.g.* adsorbed carbonate. A peak at 282 eV conforming to Ti-C, or carbon substitutionally doped in the place of oxygen in the TiO_2 lattice [19] was not observed from any of the samples.

XPS analysis of C-TNT and C,W-TNT was then carried out after sputtering the samples for 8 min with low energy Ar ions (2 keV) followed directly by sputtering for 5 min with high energy Ar ions (4 keV). The purpose of this treatment was to etch away the uppermost layers of the material. This removes any adsorbed carbonate species whose presence may be masking peaks at 282 eV related to Ti-C [19]. After sputtering, the peak at 285 eV, *i.e.* the instrumental artefact, remained in the spectra of all samples. The intensity of the C 1s peaks at 286 and 289 eV (relating to carbonate species) decreased continually upon sputtering (Figure 4). A peak at 282 eV related to Ti-C, or carbon substitutionally doped in the place of oxygen in the TiO_2 lattice [19] was finally revealed in both C-TNT and C,W-TNT. Even though this peak is relatively small (which is a reflection of the relatively low levels of carbon within the final material), it is present, and in general such low peaks in XPS spectra are as expected. . This peak was not observed in undoped P25 following similar treatment (see figure). These XPS results, as well as the bandgap measurements above, confirmed the retention of carbon as a substitutional dopant in the C-TNT and C,W-TNT samples.

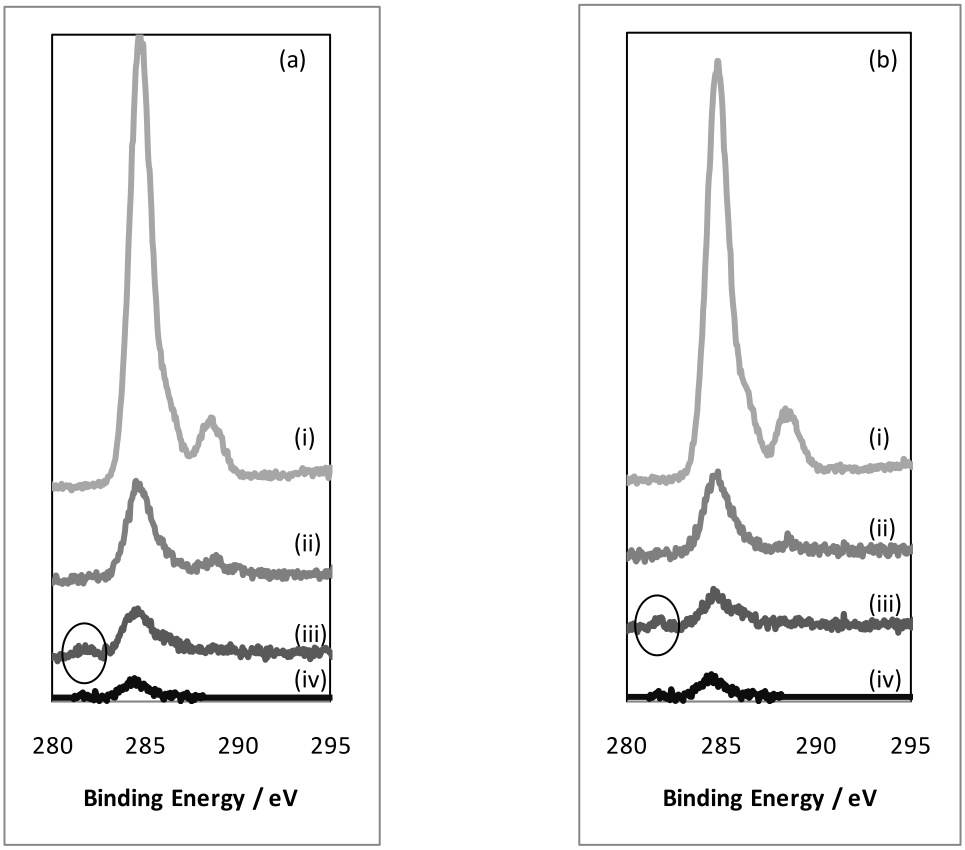

Figure 4 XPS C 1s peaks of (a) C,W-TNT and (b) C-TNT, (i) before sputtering, (ii) after sputtering with 2 keV Ar^+ ions for 8 min and (iii) after sputtering with 2 keV Ar^+ ions for 8 min and 4 keV Ar^+ ions for 5 min. (iv) P25 after sputtering.

From the C 1s peak at 282 eV, the amount of substitutional carbon dopant at the etched surface was determined. C-TNT contained 0.2 atom % substitutional carbon dopant and C,W-TNT contained 0.3 atom % substitutional carbon dopant. These values were slightly lower than the amount of substitutional carbon dopant found in the original carbon-doped TiO_2 samples, where levels of 0.5 atom % were determined (following similar etching treatments) [35]. This may explain the slight decrease in absorbance onset in the C-TNT relative to C-TiO_2 (Table 3). Carbon loss obviously resulted as a consequence of the hydrothermal treatment /acid wash. The subsequent calcination at 380 °C might also have contributed to carbon loss (*via* oxidation), if the TNT carbon dopant is less stable than the precursor TiO_2 carbon dopant (which was calcined up to 400 °C whilst still retaining 0.5 atom % C).

XPS confirmed that no Na (from the NaOH) was retained in the final TNT materials (see SI). This suggests that full ion exchange of Na^+ and H^+ occurred during HCl treatment [51] and hydrogen titanate materials were formed [48]. Also no Cl (from the HCl treatment) was detected by XPS in the final TNT materials, confirming that this too was removed during the washing step.

The W 4f and W 4d regions of the C,W-TNT XPS spectrum were then studied to investigate the nature of the W dopant in the final material (see SI). No peaks relating to W were observed (either before or after sputtering treatment) despite the precursor C,W-TiO_2 [35] displaying peaks in both the 4d region (relating to ejection of electrons from W $4d_{5/2}$ and W $4d_{3/2}$ levels at 247.2 and 259.7 eV) and in the 4f region, at 36.6 eV. XPS profiles of the Na and W regions of the spectrum are shown in the supporting information document.

The initial result does not preclude the W of the C,W-TiO_2 material existing as WO_3 clusters on, or in, the original W-doped TiO_2 nanoparticle catalyst [49] rather than atomically dispersed within its lattice as we have suggested. WO_3 readily dissolves in NaOH [50]. This means under TNT synthesis conditions (autoclaving in 10 M NaOH) the WO_3 would dissolve and remain in solution while the TNT material formed after hydrothermal synthesis was separated and washed. This would result in the absence of W in the final material, as is observed here using XPS. Another reason for the absence of W might be associated with the slightly larger atomic radius of W (1.93 Å) compared to Ti (1.76 Å) [51]. This may result in W exclusion from the titanate nanosheets formed during hydrothermal synthesis due to geometrical constraints.

The absence of W in C,W-TNT explains why the optical properties (and the surface area) of C,W-TNT were so similar to those of C-TNT (Figure 3 and Tables 2 and 4), since both materials contained carbon dopant only.

We can conclude that carbon dopants in TiO_2 are retained after hydrothermal TNT synthesis as long as they are substitutionally doped into the lattice of the TiO_2. We believe this is the first example of C-doping in a TNT material remaining from C-doping in a nanoparticulate starting material. The fact that W atoms are not transferred to the formed titanates in a similar way shows that the technique is not universally applicable.

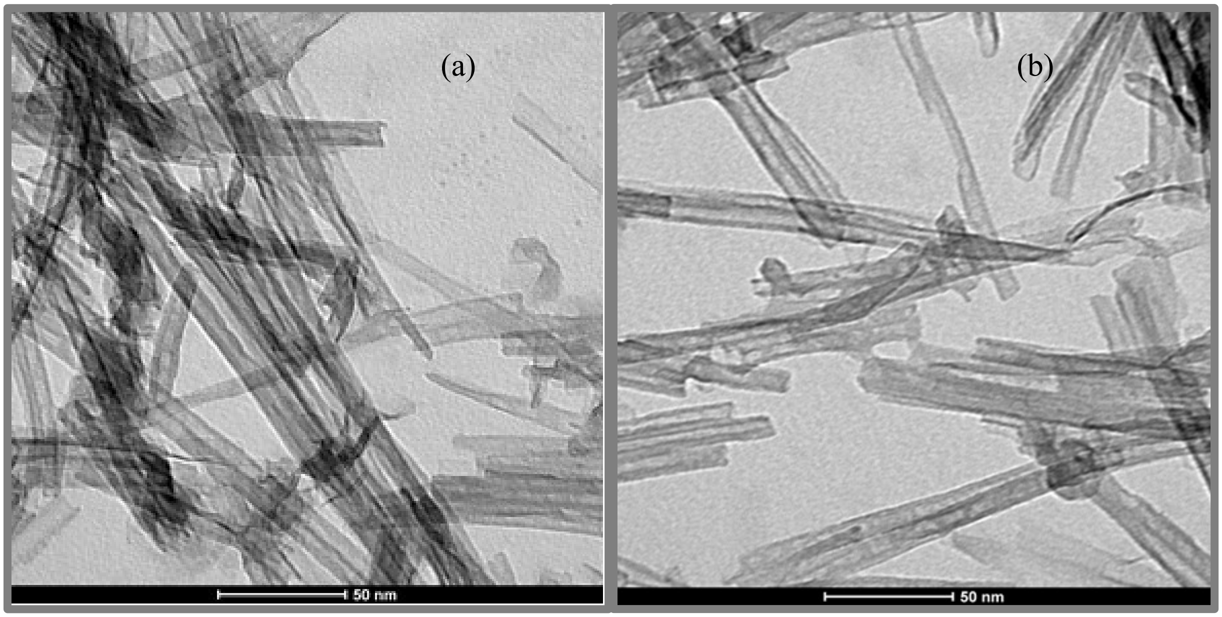

Figure 5 TEM images of TNT (a) and C-TNT (b)

3.5 Transmission Electron Microscopy

TEM (Figure 5) revealed the formation of well dispersed nanotubes ranging from 100 – 400 nm in length for both TNT and C-TNT materials. Carbon doping of the nanotubes did not dramatically affect their size or structure. TNT had an average diameter of 7.1 ± 1.3 nm and C-TNT had an average diameter of 7.3 ± 1.5 nm in diameter (in each case the diameters of 50 nanotubes were measured to determine this value).

Using the pore radii calculated from N_2 physisorption analysis (1.6 nm for both TNT and C-TNT, Table 2) and the outer diameters measured using TEM, we can estimate the wall thickness to be ~2.0 nm for TNT and ~2.1 nm for C-TNT. These diameters and wall sizes are in good agreement with the morphologies previously reported for hydrothermally synthesized TNTs [14, 17, 52].

	% conversion	
	Nanoparticulate	Titanate
P25	7.0	24.3
C-TiO_2	18.0	36.1
C,W-TiO_2	11.1	31.4

Table 4. The photocatalytic degradation of 4-chlorophenol under visible light (for 1 h) by P25 and C-TiO_2 nanoparticulate materials and their analogous titanates.

3.6 Photocatalytic activity

The initial photocatalytic activity of the materials was tested by investigating the photocatalytic degradation of 4-chlorophenol solutions under visible light irradiation. Samples were extracted after 1 hour and the degradation (complete mineralisation) of 4-chlorophenol was determined using TOC analysis.

Table 4

The photocatalysis results are shown in Table 4. C-TNT was the most active catalyst, degrading over 35 % of the 4-chlorophenol (as measured using TOC) in 1 hour. C-TNT degraded significantly more 4-chlorophenol than TNT which removed only 24 % and P25 which degraded less than 10 %.

As seen previously [35] C,W-TiO_2 was less active than the C-TiO_2 under these conditions (due to the action of W as an electron hole recombination centre), and notwithstanding the fact that XPS has shown that W was removed during the titanate formation the resulting titanate material (C,W TNT) is still less active than C-TNT. These materials have similar surface areas, so this feature might relate to crystallinity (recall XRD has shown the C-TNT to be less crystalline than the C,W-TNT.

In general, titanate materials are more active than their nanoparticulate analogues, and C-containing materials are more active than their C-free analogues. This could be due to the enhanced optical properties of the C-containing materials relative to the C-free analogues (where more visible photons were absorbed (Figure 3)).

TNT performed better than its nanoparticulate analogue, P25 (Degussa). The optical properties of these two materials were similar and therefore the increased photoactivity observed was probably due to the other reported enhanced photocatalyst properties such as increased surface area, improved charge transfer and charge separation properties possessed by the TNT material [11]. The increased surface area of the nanotube materials relative to the nano-particulates might also play a role here (Table 2).

C-TNT also performed better than its nanoparticulate analogue C-TiO_2 which degraded ~ 18 % of the 4-chlorophenol in the allotted time period, despite the enhanced optical absorbance of the latter. This suggests again that characteristics such as higher surface area, enhanced charge separation and transfer, possessed by the TNT materials [11], can outweigh the benefits associated with the improved visible absorbance possessed by nanoparticulate C-TiO_2.

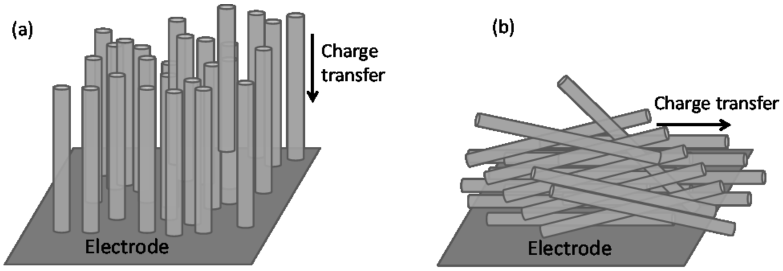

Figure 6 Schematic of nanotubes (a) optimally aligned on an electrode surface with efficient charge transfer to the electrode and (b) electrode non-optimally aligned

3.7 Photocurrent measurements

Photocurrent measurements have been carried out to determine photon to current conversion abilities of selected photocatalysts. C-TNT, C-TiO_2 and the benchmark photocatalyst P25 TiO_2 were analyzed using this technique. These chosen materials were screen printed onto conducting glass (FTO) substrates and their photocurrent densities recorded upon simulated solar light irradiation (AM 1.5 G) using a solar simulator.

From the photocurrent measurements (Figure 7) we found that, under irradiation, C-TNT generated a lower photocurrent density across the range of applied potential than both C-TiO_2 and TNT. The result was initially surprising as C-TNT was the most active of these materials photocatalytically (Table 4). However, it should be recalled that, due to the nanoscale cross-section of the C-TNT material, electrons propagate most efficiently along the tube's axis (*i.e.* it is

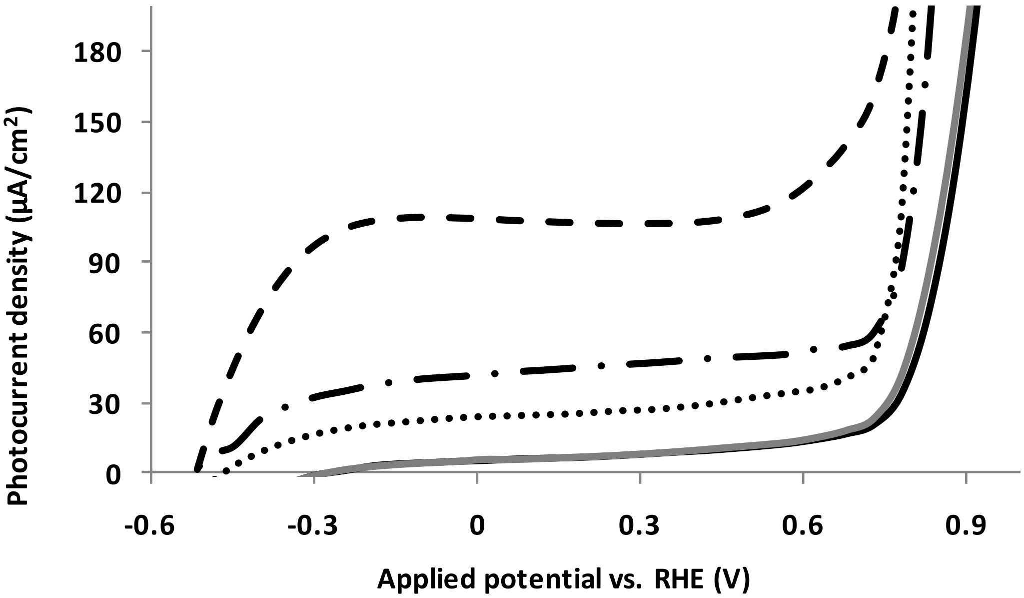

Figure 7 Photocurrent density measurements of P25 (dotted line), C-TiO_2 (dashed line), C,W-TiO_2 (dots and dashes), C,W-TNT (grey line) and C-TNT (black line) photo-electrodes.

a one-dimensional conductor) [52]. This means that if the nanotubes are not vertically aligned to the surface of the electrode, the transfer of generated electrons to the electrode is severely compromised (see Figure 6). This results in a reduction in measurable photocurrent. For the nanoparticulate materials (P25 and C-TiO_2), orientation on the electrode surface is not as important and so the screen printing method of photocatalyst immobilization is suitable. Screen printing of TNTs appears to result in a non-ordered arrangement of the TNTs on the electrode surface, which is responsible for the decreased photocurrent response of C-TNT. This is represented in Figure 7.

Consequently, there has been much research recently focused on the formation of ordered arrays of TNTs [7, 17, 53]. This is important for TNT in many areas such as photoelectrochemical water splitting [54] and dye sensitised solar cells [55]. But as we have seen, for photocatalytic degradation of pollutants in a liquid medium under visible light, dispersed non-ordered TNTs have great potential as solar driven photocatalysts.

4 Conclusions

We have formed carbon-doped titanate nanotubes (C-TNT) *via* the hydrothermal treatment of a pre-doped TiO_2 powder (C-TiO_2), thus demonstrating the potential to form substitutionally doped TNTs from pre-formed substitutionally doped TiO_2 materials. To our knowledge this has not been previously demonstrated. Substitutional carbon doping of the TNT was verified by XPS and results in improved visible absorbance relative to un-doped TNT materials.

Attempts were made to form W containing TNTs (C,W-TNT) from a nanoparticulate C and W co-doped precursor (C,W-TiO_2). However, W was not detected by XPS in the final TNT material and the improved optical and surface area properties associated with W co-doping of the nanoparticles was not evident in the TNT material. This indicates that W was present in these nanoparticulate materials as soluble WO_3 or that exposed W atoms in an anatase lattice are themselves susceptible to solvation (possibly due to the size of the W atom). Furthermore, this indicates that the technique is not universal and future work will study the limitations involved with transferring dopants from nanoparticles (where they can be easily inserted using modified sol-gel processes) to titanate nanotubes.

The TNT materials XRD profiles displayed titanate phase peaks as opposed to the predominantly anatase phase or their TiO_2 particulate precursors. As expected, the TNT materials had higher surface areas relative to their particulate precursors and were ~7 nm in diameter and in excess of 100 nm in length (as shown using TEM).

The TNT materials displayed reduced absorbance in the visible region compared to their TiO_2 particulate precursors. However, carbon doped C-TNT displayed an enhanced optical absorbance compared to both TNT and nanoparticulate P25.

The TNT materials also displayed enhanced photocatalytic activities compared to their nanoparticulate analogues. C-TNT displayed enhanced photocatalytic activity compared to TNT, P25 and its nanoparticulate analogue (C-TiO_2). Photocurrent measurements showed C-TNT to be less effective than nanoparticulate P25 when screen printed on electrode surfaces. This is believed to be due to non-optimal alignment of the TNTs on the electrode surface and highlights the importance of research into different methods to form ordered arrays of such nanotubes for photoelectrode-based applications.

5 Acknowledgements.

We acknowledge and thank Science Foundation Ireland for their funding of this Strategic Research Cluster Programme (07/SRC/B1160) and our Industry Partners for their support of this Cluster. We specifically thank SSE Renewables for their support of E.M.N. we are also grateful to Anne-Katrin Prescher for assistance with TOC analysis.

This article is dedicated to the memory of Prof. Joseph Cunningham, Department of Chemistry, UCC, Cork, Ireland

6 References

[1] T. Kasuga, M. Hiramatsu, A. Hoson, T. Sekino and K. Niihara, Langmuir, 14 (1998) 3160-3163.

[2] T. Kasuga, M. Hiramatsu, A. Hoson, T. Sekino and K. Niihara, Advanced Materials, 11 (1999) 1307-1311.

[3] D.V. Bavykin, J.M. Friedrich and F.C. Walsh, Advanced Materials, 18 (2006) 2807-2824.

[4] D. Gong, C. Grimes, O.K. Varghese, W. Hu, R. Singh, Z. Chen and E.C. Dickey, Journal of Materials Research, 16 (2001) 3331-3334.

[5] O.K. Varghese, D. Gong, M. Paulose, C.A. Grimes and E.C. Dickey, Journal of Materials Research, 18 (2003) 156-165.

[6] J.H. Lee, I.C. Leu, M.C. Hsu, Y.W. Chung and M.H. Hon, The Journal of Physical Chemistry B, 109 (2005) 13056-13059.

[7] P. Hoyer, Langmuir, 12 (1996) 1411-1413.

[8] G. Du, Q. Chen, R. Che, Z. Yuan and L.M. Peng, Applied Physics Letters, 79 (2001) 3702.

[9] S. Zhang, L.M. Peng, Q. Chen, G. Du, G. Dawson and W. Zhou, Physical Review Letters, 91 (2003) 256103.

[10] C.C. Tsai and H. Teng, Chemistry of Materials, 16 (2004) 4352-4358.

[11] M. Grandcolas, A. Louvet, N. Keller and V. Keller, Angewandte Chemie, 121 (2009) 167-170.

[12] D. Wu, J. Liu, X. Zhao, A. Li, Y. Chen and N. Ming, Chemistry of Materials, 18 (2006) 547-553.

[13] Q. Chen, G. Du, S. Zhang and L.M. Peng, Acta Crystallographica Section B: Structural Science, 58 (2002) 587-593.

[14] D.V. Bavykin, V.N. Parmon, A.A. Lapkin and F.C. Walsh, J. Mater. Chem., 14 (2004) 3370-3377.

[15] B. Yao, Y. Chan, X. Zhang, W. Zhang, Z. Yang and N. Wang, Applied Physics Letters, 82 (2003) 281-283.

[16] W. Wang, O.K. Varghese, M. Paulose, C.A. Grimes, Q. Wang and E.C. Dickey, Journal of Materials Research, 19 (2004) 417-422.

[17] H.H. Ou and S.L. Lo, Separation and Purification Technology, 58 (2007) 179-191.

[18] S.U.M. Khan, M. Al-Shahry and W.B. Ingler, Science, 297 (2002) 2243-2245.

[19] J. Yu, T. Ma, G. Liu and B. Cheng, Dalton Transactions, 2011, 40, 6635-664.

[20] T. Tachikawa, S. Tojo, K. Kawai, M. Endo, M. Fujitsuka, T. Ohno, K. Nishijima, Z. Miyamoto and T. Majima, The Journal of Physical Chemistry B, 108 (2004) 19299-19306.

[21] J. Yu, T. Ma, G. Liu and B. Cheng, Dalton Transactions, 2011, 40, 6635-664.

[22] T. Ikeda, T. Nomoto, K. Eda, Y. Mizutani, H. Kato, A. Kudo and H. Onishi, The Journal of Physical Chemistry C, 112 (2008) 1167-1173.

[23] R. Asahi, T. Morikawa, T. Ohwaki, K. Aoki and Y. Taga, Science, 293 (2001) 269-271.

[24] O. Lorret, D. Francova, G. Waldner and N. Stelzer, Applied Catalysis B-Environmental, 91 (2009) 39-46.

[25] C. Huang, X. Liu, L. Kong, W. Lan, Q. Su and Y. Wang, Applied Physics A: Materials Science & Processing, 87 (2007) 781-786.

[26] H. Tokudome and M. Miyauchi, Chemistry Letters, 33 (2004) 1108-1109.

[27] J. Geng, D. Yang, J. Zhu, D. Chen and Z. Jiang, Materials Research Bulletin, 44 (2009) 146-150.

[28] H. Cheng-Ching, H. Tzu-Chien and K. Li-Heng, International Journal of Photoenergy, 2012 (2011).

[29] C.H. Rhee, J.S. Lee and S.H. Chung, Journal of Materials Research, 20 (2005) 3011-3020.

[30] A.M. Milad, M.B. Kassim and W.R. Daud, World Academy of Science Engineering and Technology, (2011) 171-175.

[31] J.H. Park, S. Kim and A.J. Bard, Nano Letters, 6 (2006) 24-28.

[32] R. Hahn, A. Ghicov, J. Salonen, V.P. Lehto and P. Schmuki, Nanotechnology, 18 (2007) 105604.

[33] C.W. Lai and S. Sreekantan, Journal of Alloys and Compounds 547 (2013) 43–50.

[34] Q. Xiao and L. Ouyang, Journal of Physics and Chemistry of Solids,72 (2011) 39–44.

[35] E.M. Neville, M.J. Mattle, D. Loughrey, B. Rajesh, M. Rahman, J.M.D. MacElroy, J.A. Sullivan and K.R. Thampi, The Journal of Physical Chemistry C, 116 (2012) 16511–16521.

[36] M. Grandcolas, A. Louvet, N. Keller and V. Keller, Angewante Chemie International Edition, 48 (2009) 161-164.

[37] S. Ito, P. Chen, P. Comte, M.K. Nazeeruddin, P. Liska, P. Péchy and M. Grätzel, Progress in Photovoltaics: Research and Applications, 15 (2007) 603–612.

[38] Y. Niu, M. Xing, B. Tian and J. Zhang, Applied Catalysis B: Environmental, 115 (2012) 253.

[39] G.S. Kim, Y.S. Kim, H.K. Seo and H.S. Shin, Korean Journal of Chemical Engineering, 23 (2006) 1037-1045.

[40] H.Y. Zhu, Y. Lan, X.P. Gao, S.P. Ringer, Z. Zheng, D.Y. Song and J.C. Zhao, Journal of the American Chemical Society, 127 (2005) 6730-6736.

[41] L. Xiong, Y. Yang, J. Mai, W. Sun, C. Zhang, D. Wei, Q. Chen and J. Ni, Chemical Engineering Journal, 156 (2010) 313-320.

[42] S. Mozia, E. Borowiak-Palen, J. Przepiórski, B. Grzmil, T. Tsumura, M. Toyoda, J. Grzechulska-Damszel and A.W. Morawski, Journal of Physics and Chemistry of Solids, 71 (2010) 263-272.

[43] X. Lin, F. Rong, X. Ji, D. Fu and C. Yuan, Solid State Sciences, 13 (2011) 1424-1428.

[44] E. Papirer, R. Lacroix, J.B. Donnet, G. Nanse and P. Fioux, Carbon, 33 (1995) 63-72.

[45] Y. Li, Y. Fan and Y. Chen, Journal of Materials Chemistry, 12 (2002) 1387-1390.

[46] T. Ohno, T. Tsubota, K. Nishijima and Z. Miyamoto, Chemistry Letters, 33 (2004) 750-751.

[47] S. Sakthivel and H. Kisch, Angewandte Chemie-International Edition, 42 (2003) 4908-4911.

[48] M. Zhou and H. Yu, International Journal of Photoenergy, 2012 (2012).

[49] S.Y. Chai, Y.J. Kim and W.I. Lee, Journal of Electroceramics, 17 (2006) 909-912.

[50] S. Astha, R. Balasubramaniam and A. Paranipe, Journal of Materials Science Letters, 18 (1999) 1555-1556.

[51] R.F. Bryan, Acta Crystallographica Section B: Structural Science, 51 (1995) 893-894.

[52] J.C. Charlier, X. Blase and S. Roche, Reviews of Modern Physics, 79 (2007) 677.

[53] K. Shankar, M. Paulose, G.K. Mor,O.K. Varghese and C.A Grimes, J. Phys. D: Appl. Phys. 38 (2005) 3543–3549

[54] G.K. Mor, K. Shankar, M. Paulose, O.K. Varghese and C.A. Grimes, Nano Letters, 5 (2005) 191-195.

[55] G.K. Mor, K. Shankar, M. Paulose, O.K. Varghese and C.A. Grimes, Nano Letters, 6 (2006) 215-218.

S1

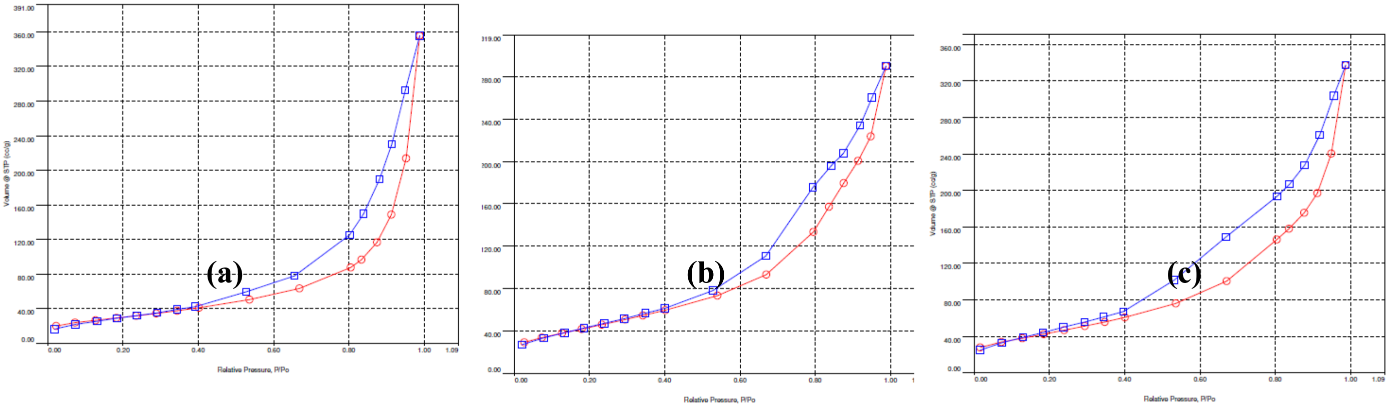

Figure S1: Typical BET Isotherms for (a) TNT, (b) CTNT and (c) C,W TNT. Adsorption profiles (○), desorption profiles (□).

S2

W 4d **W 4f**

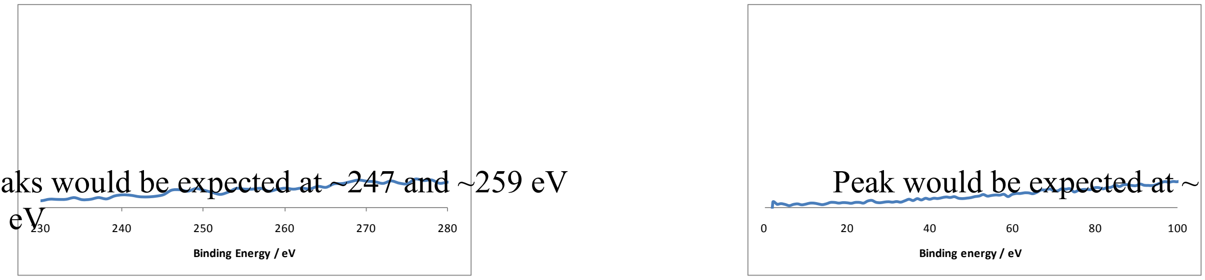

Peaks would be expected at ~247 and ~259 eV

Peak would be expected at ~ 36 eV

Na 1s **Na Auger**

Peak would be expected at ~ 1080 eV

Peak expected at ~ 496 eV

S2 XPS data showing absence of peaks relating to W and Na in nanotubes formed following hydrothermal treatment of C,W-TiO_2 .

S3

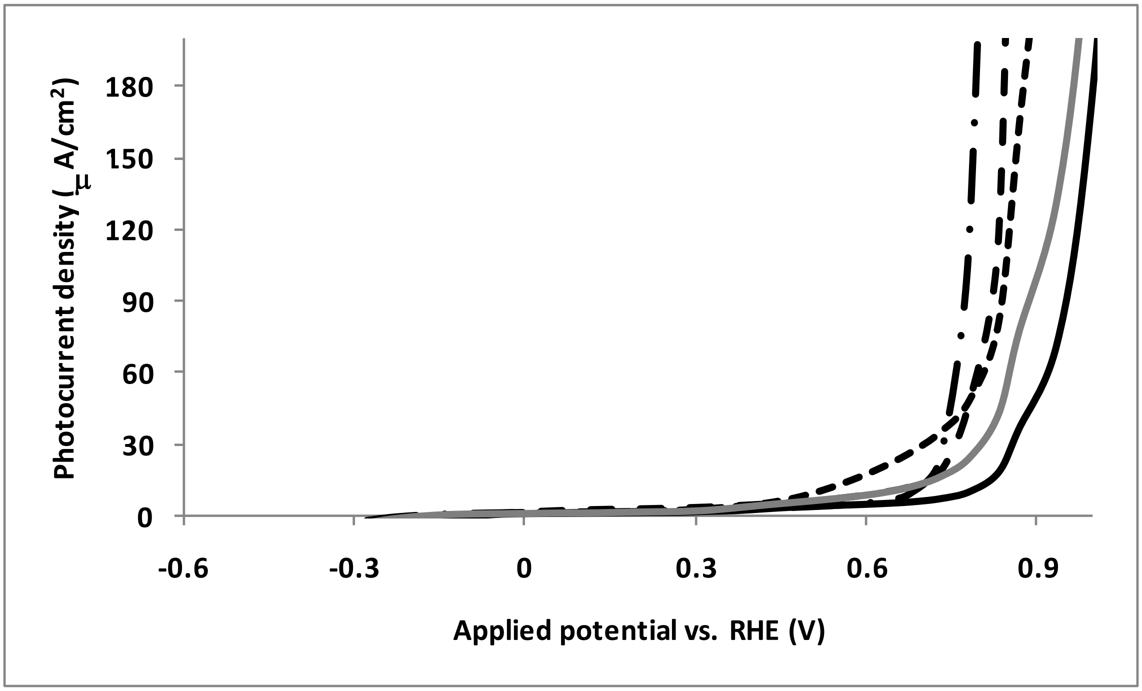

S3 dark current iV measurements of P25 (dotted line), C-TiO$_2$ (dashed line), C,W-TiO$_2$ (dots and dashes), C,W-TNT (grey line) and C-TNT (black line) photo-electrodes